Top Catal (2010) 53:210–217
DOI 10.1007/s11244-009-9413-z

ORIGINAL PAPER

Highly Stable Amine-modified Mesoporous Silica Materials for Efficient CO_2 Capture

Shou-Heng Liu · Chia-Hua Wu · Huang-Kuei Lee · Shang-Bin Liu

Published online: 1 December 2009

Abstract A highly efficient and stable solid adsorbent invoking a direct incorporation of tetraethylenepentamine (TEPA) onto the as-synthesized mesocelullar silica foam (MSF) has been developed for CO_2 capture. Unlike most amine-functionalized silicas, which typically exhibit CO_2 adsorption capacities less than 2.0 mmol/g, such organic template occluded mesoporous silica-amine composites exhibited remarkably high CO_2 uptake as high as 4.5 mmol/g at 348 K and 1 atm. Moreover, notable increases in CO_2 adsorption capacities of the composite materials were observed when in the presence of humidity. Durability test performed by cyclic adsorption–desorption revealed that such adsorbents also possess excellent stability, even though a slight decrease in adsorption capacity over time was observed.

Keywords Amine · Surface functionalization · Mesoporous silica · Mesocellular silica foam · CO_2 capture

S.-H. Liu · C.-H. Wu · S.-B. Liu (✉)
Institute of Atomic and Molecular Sciences, Academia Sinica, Taipei 10617, Taiwan
e-mail: sbliu@sinica.edu.tw

C.-H. Wu · H.-K. Lee
Institute of Materials Science and Nanotechnology, Chinese Culture University, Taipei 11114, Taiwan

Present Address:
S.-H. Liu
Department of Chemical and Materials Engineering, National Kaohsiung University of Applied Sciences, Kaohsiung 80778, Taiwan

1 Introduction

In a view of the increasing concerns in global environmental issues, such as suppressions of greenhouse gases and global warming, carbon sequestration has becoming a demanding and challenging research topic [1, 2]. In particular, research and development for cost-effective 'scrubbing' (i.e., separation and capture) of CO_2 remains one of the most crucial tasks in carbon sequestration. Current available CO_2 separation schemes normally invoke absorption by a liquid, adsorption by a solid, or separation by selective transport, for example, through a membrane [3]. However, these schemes are generally limited by the high capital and operation costs, particularly when applied for fossil fuel combustion (low pressure) or gasification (high pressure) streams. The high costs for these schemes mostly arise from low mass fluxes in the separation units, production of a high-pressure steam, and high-energy consumption during regeneration of the adsorbents. Thus, to make any process economically attractive, crucial issues such as cost, operation life, and selectivity of the separation agents, and complexity of the process invoked must be considered.

At present, available commercial processes for CO_2 absorption mostly utilize technologies based on chemical absorption by alkanolamines, including the primary (e.g., monoethanolamine; MEA), secondary (e.g., diethanolamine; DEA), and tertiary (e.g., methyldiethanolamine; MDEA) amines [4–8]. Upon absorption, primary and secondary amines are known to react rapidly with CO_2 to form carbamates and that the addition of a purely physical solvent such as water, tend to enhance the CO_2 absorption capacity and rate by many folds. However, since the formation of carbamate ions is normally associated with a relatively high heat of absorption, the cost of regenerating primary and secondary amines is high. Moreover, these

amines also have the disadvantage that the stoichiometry is 2:1 and hence their loadings are limited to 0.5 mole of CO_2 per mole of amine. Tertiary amines lack the N-H bond required to form the carbamate ion and therefore do not react directly with CO_2. However, in aqueous solutions, tertiary amines promote the hydrolysis of CO_2 to form bicarbonate and protonated amines. Nevertheless, in addition to high-energy consumption, such liquid amine-based CO_2 separation processes also suffer from severe drawbacks, such as solvent deterioration, equipment corrosion, and limited amine concentration in the aqueous phase due to viscosity and foaming issues [1, 2]. Although several new processes such as absorption/adsorption by solid absorbents/adsorbents, membrane and cryogenic separation have been developed to tackle these problems, aiming at lowering the energy consumption and equipment cost, and more versatile operation conditions, most of them are still far from practical industrial applications.

Removal of CO_2 from a gas stream normally invokes operation carried out at high temperatures (typically, >700 °C) in a combustion process. Among various chemical absorbents, metal oxides [9–12], Li-containing zirconates [13–17] and poly-ionic liquids [18, 19] have been investigated. Numerous studies have explored methods of physisorption using functionalized/modified nanoporous solids for the abatement of CO_2, for examples, microporous zeolites [20–26], activated carbons [27–29], porous coordination polymers or organic nanostructure materials [30–32]. However, these materials normally exhibit low CO_2 adsorption capacity (typically smaller to the benchmark value of ca. 2.0 mmol per gram adsorbent for practical commercialization) except for alkali ion-exchanged faujasite (X, Y) zeolites [24] and high surface area activated carbon materials (Maxsorb^{TM}) [27] which were found to have CO_2 uptake capacities up to 10–13 mmol/g. Nevertheless, these materials tend to suffer from problems such as low capacity, poor selectivity, poor tolerance to water, and high-temperature regeneration or activation. The effects of water on the adsorption of CO_2 on various adsorbents have been examined [33]. In addition, some recent studies have shown that metal-organic framework (MOFs) [34–37] and van der Waals crystals [38] are potential CO_2 adsorbents.

Ordered mesoporous silica (OMSs) and carbon materials with tunable pore size (2–50 nm), narrow pore size distribution, high surface area, large pore volume, and good thermal stability are particularly attractive for applications as gas adsorbents. Many studies using OMSs as CO_2 adsorbents have been investigated [39–63]. The pore surfaces of OMSs are enriched with hydroxyl groups, which facilitate direct or post-synthesis grafting of organic functional groups. Such mesostructured porous organic-inorganic hybrid materials with synergistic effects provoked by tailored pore structures, connectivity, and particle size may offer additional advantages of being multifunctional, which make possible for engineering the chemical environments of the binding sites. For CO_2 capture, the most interesting organic functional groups would be polyamines compounds that possess high amine group density (large amount of CO_2 sorption sites) and slow CO_2 adsorption/desorption kinetics. Amine-functionalized mesoporous materials, therefore, provide concrete objective criteria to act as the CO_2 "molecular basket" adsorbents, which facilitates a synergic effect on the CO_2 adsorption capacity and adsorption kinetic between nanoporous supports and polyamines (especially at high polyamine loading). For example, for the polyethylenimine (PEI)-impregnated MCM-41, a high CO_2 adsorption capacity of 246 mg/g-PEI was obtained with a PEI loading of ca. 50 wt%, which is 30 times higher than that of MCM-41 and is about 2.3 times that of the neat PEI [43–46]. Several other different types of polyamines grafted on various OMSs, such as MCM-41, MCM-48, SBA-15 etc. have been examined for CO_2 adsorption [41, 47–58]. Unfortunately, their CO_2 adsorption capacities were normally below the benchmark value of 2.0 mmol/g. Recently, Sayari and co-workers incorporated amines into the nanoporous MCM-41 silicas, allowing them to be used in both wet and dry environments, potentially eliminating significant engineering challenges. Owing to its very large pore volume, the DEA loaded on pore-expanded PE-MCM-41 [59–63] was capable of 'scrubbing' CO_2 in a higher quantity of amine and more resistant to moisture compared with the other supports including activated carbon, silica gel, and MCM-41 silica. Repeated adsorption-desorption cycles revealed that these novel materials exhibited much better cyclic stabilities than typical zeolite absorbents [59].

In this study, two different methods have been adopted to prepare amine-functionalized adsorbent materials, namely (i) by incorporating 3-[2-(2-Aminoethylamino)ethylamino]-propyltrimethoxysilane (TA) and N-[3-(Trimethoxysilyl) propyl]ethylenediamine (APS) onto mesoporous silica SBA-15 [64] and mesocellular silica foam (MSF) [65] and (ii) by directly incorporating tetraethylenepentamine (TEPA) onto the as-synthesized MSF without removing the organic templates. These amine-functionalized porous materials were characterized by a variety of different analytical and spectroscopic techniques, such N_2 adsorption/desorption, X-ray diffraction (XRD), elemental analysis (EA), Fourier-transformed infrared (FTIR), and thermogravimetric analysis (TGA). Among them, the absorbents prepared by the latter method not only represent a time-saving route in terms of material preparation but also superior CO_2 adsorption capacity and durability after repeated adsorption-desorption cycles, revealing some opportunities for future practical applications.

2 Experimental

2.1 Materials Preparation

The parent SBA-15 and MSF materials were synthesized according to recipes documented in the literatures [64, 65]. Typically, for the synthesis of SBA-15, 5.7 g of neutral triblock co-polymer surfactant, Pluronic 123, was dissolved in a mixture of 37% HCl solution (24.4 g) and water (169.3 g) at room temperature (295 K). After adding tetraethyl orthosilicate (TEOS), the resulting mixture was stirred at 313 K for 20 h and then transferred into a polypropylene bottle and reacted at 373 K under static condition for 24 h. For the preparation of MSF samples, 4 g of Pluronic 123 was dissolved in 150 mL of aqueous 1.6 N HCl at room temperature, then, 23 mg of NH_4F and 3 g of trimethylbenzene (TMB) were added into the mixture. After stirring for 1 h at 313 K, 8.5 g of TEOS was added to the mixture. The resulting reaction mixture was stirred at 313 K for 20 h followed by aging at 373 K for 24 h. The solid products of as-synthesized SBA-15 and MSF were recovered by filtration and dried at room temperature overnight followed by removal of organic template by calcination at 823 K. TA- and APS-functionalized SBA-15 and MSF materials (denoted as TA-SBA-15, APS-SBA-15, TA-MSF, and APS-MSF, respectively) were prepared by the post-synthesis grafting method. Typically, calcined SBA-15 or MSF (0.25 g) was first dried at 398 K for 6 h in air, then, refluxed in toluene solution (12 mL) of aminosilane (2.1 mL) at 383 K for 24 h under an N_2 flow. The product was washed with toluene and dried at 333 K over night.

Alternatively, tetraethylenepentamine (TEPA) incorporated on the as-synthesized MSF materials (i.e., in the presence of organic templates; denoted as MSFas) were also prepared. This was carried out by dissolving a known amount of TEPA in 10 g of ethanol under stirring for 0.5 h, and then 0.2 g of MSFas was added into the solution. After stirring and refluxing for 2 h, the mixture was evaporated at 353 K, followed by drying at 373 K for 1 h. The final products were obtained (denoted as TEPA-MSFas-x, where x represents the amount of N in wt%) after filtration, washing with water, and then drying in air at room temperature.

2.2 Characterization Methods

X-ray diffraction (XRD) patterns were recorded on a PANalytical (X'Pert PRO) instrument using Cu Kα radiation ($\lambda = 0.1541$ nm). Elemental analyses (EA) were carried out using a CHN elemental analyzer (Heraeus CHN-O-S-Rapid). Nitrogen adsorption/desorption isotherms were measured at 77 K on a Quantachrome Autosorb-1 volumetric adsorption analyzer. Fourier transform infrared (FTIR) spectra were collected on a Bruker IFS-28 FTIR spectrometer with 4 cm^{-1} resolution using KBr pellets at room temperature.

2.3 CO_2 Adsorption Capacity Measurements

To assess the adsorption and desorption properties of various adsorbents, a modified thermogravimetric analyzer (TGA, Netzsch TG209) with a H_2O saturator (Fig. 1) was used. In a typical adsorption/desorption process, ca. 10 mg of adsorbent placed in a sample cell was heated to 373 K under N_2 flow (50 mL/min), then, maintained at that temperature for ca. 30 min till no further weight loss was observed. Subsequently, the sample was then cooled down to 348 K and 15% dry CO_2 was introduced at a flow rate of 50 mL/min. After adsorption, the gas was switched to pure N_2 flow (50 mL/min) to proceed desorption procedure at the same temperature. The time required for each adsorption and desorption cycle was 120 min. The influence of moisture on CO_2 adsorption capacities was also investigated together with cyclic adsorption/desorption measurements to evaluate the stability of the adsorbents.

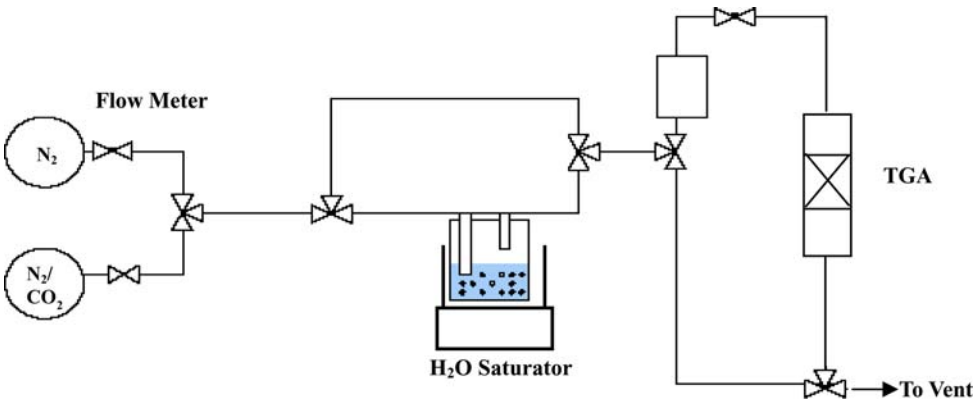

Fig. 1 Schematic diagram of the CO_2 adsorption system

3 Results and Discussion

The small-angle XRD profiles of the parent and amine-functionalized SBA-15 samples are shown in Fig. 2a. The parent SBA-15 exhibited a main intensive (100) peak at 2θ of ca. 0.9° and two weak (110) and (200) diffraction peaks, indicating the existence of well-ordered hexagonal arrays and two-dimensional (2D) channel structure. However, upon incorporating APS and TA onto the matrix, notable decreases in diffraction peak intensities were observed. The N_2 adsorption/desorption curves (Fig. 2b) of the parent SBA-15 sample showed typical type IV isotherms with a well defined hysteresis loop, revealing the presence of ordered mesopores in the frameworks, in agreement with XRD result. The diminishing of hysteresis loop upon introducing amine functional group may be ascribed due to blockage of the mesopore channels. As shown in Table 1, notable decreases in pore volume and surface area were observed for amine-functionalized samples compared to the parent SBA-15. Likewise, the uniformity of MSF mesostructure was also confirmed by the XRD peak at 2θ of ca. 0.5° (Fig. 3a). The BET surface area (S_{BET}), total pore volume (V_{tot}), and BJH pore size (D_{BJH}) derived from N_2 adsorption/desorption isotherms for the parent and amine-functionalized MSF samples (Fig. 3b) are also summarized in Table 1. Since the MSF sample possesses a much larger pore volume (2.68 cm^3/g) and pore size (23 nm) than the parent SBA-15 (V_{tot} = 1.86 cm^3/g; D_{BJH} = 10 nm), some mesoporosities remained available even after loading of a substantial amount of aminosilane onto the sample, as revealed by the existence of hysteresis loop in the isotherm of both APS-MSF and TA-MSF samples (Fig. 3b). The presence of amine functional groups in the surface-modified SBA-15 and MSF samples was further confirmed by FTIR spectroscopy, as shown in Figs. 2c and 3c. Compared with their parent counterparts, additional feature peak at 1510 cm^{-1} and a broad band

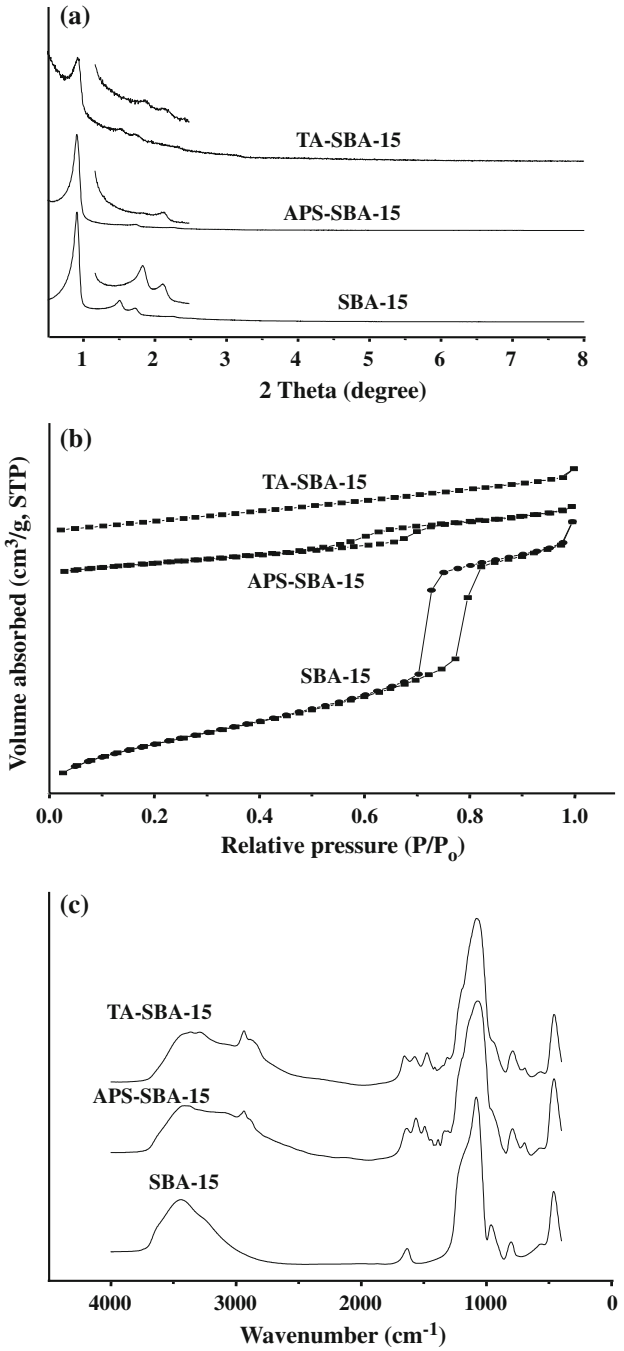

Fig. 2 **a** XRD patterns, **b** N_2 adsorption-desorption isotherms, and **c** FTIR spectra of SBA-15, APS-SBA-15, and TA-SBA-15

Table 1 Textural properties of parent and amine-functionalized SBA-15 and MSF samples

Sample	N content (wt%)[a]	V_{tot} (cm^3/g)[b]	S_{BET} (m^2/g)[c]	D_{BJH} (nm)[d]
SBA-15	—	1.9	1080	10
APS-SBA-15	5.6	0.4	250	7
TA-SBA-15	9.5	0.4	399	3
MSF	—	2.7	901	23
APS-MSF	4.7	1.3	407	18
TA-MSF	5.6	0.7	139	18
MSFas	—	0.4	54	N/A
TEPA-MSFas-0.6	0.6	0.3	34	N/A
TEPA-MSFas-7.5	7.5	0.3	39	N/A
TEPA-MSFas-8.9	8.9	0.2	30	N/A
TEPA-MSFas-13.7	13.7	~ 0.1	16	N/A
TEPA-MSFas-18.1	18.1	~ 0.1	12	N/A

[a] Nitrogen content measured by elemental analysis

[b] Total pore volumes calculated as the amount of N_2 adsorbed at P/P_o = 0.99

[c] Brunauer–Emmet–Teller (BET) surface areas

[d] Pore diameters calculated by the Barrett–Joyner–Halenda (BJH) method using the adsorption branches

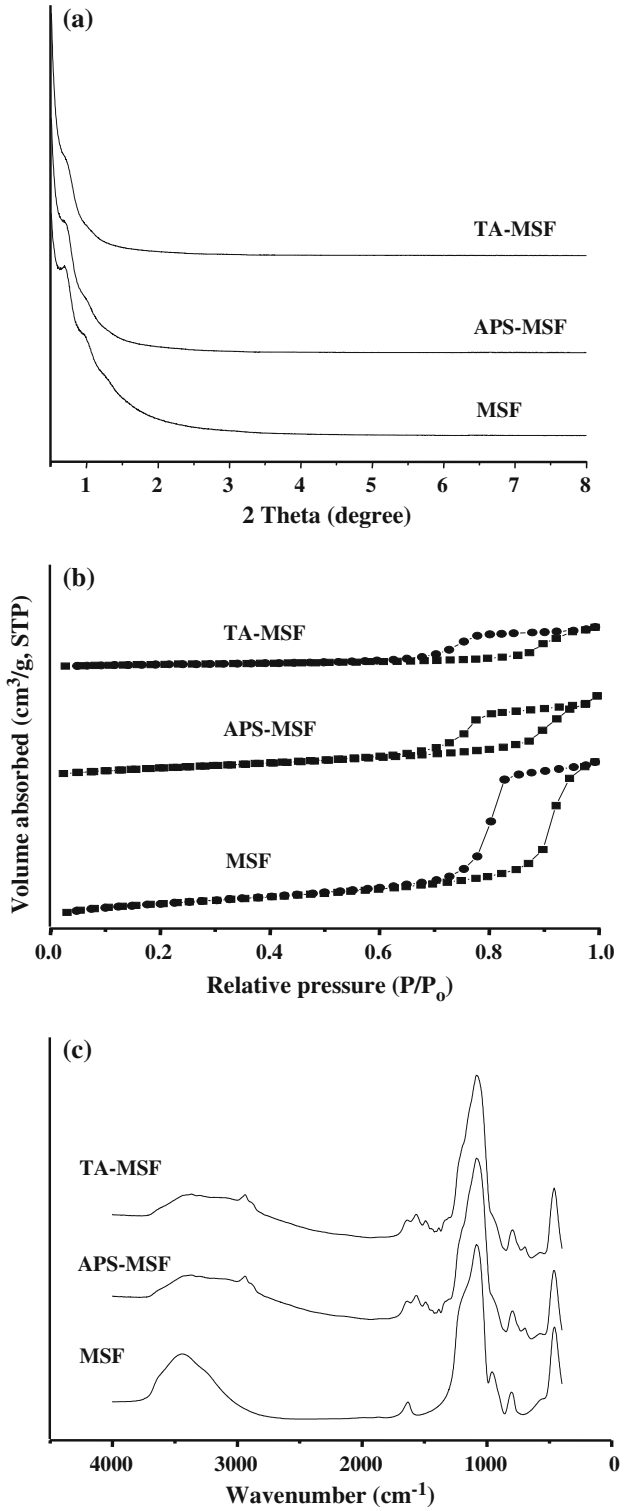

Fig. 3 **a** XRD patterns, **b** N_2 adsorption-desorption isotherms, and **c** FTIR spectra of MSF, APS-MSF, and TA-MSF

at 2700–3400 cm^{-1} were evident for TA- and APS-modified SBA-15 and MSF samples, which may be assigned due to symmetric NH_2 bending vibration and NH^+ stretching vibration, respectively. Further analyses by EA data revealed that the nitrogen contents in those amine-functionalized samples vary from 4.7 to 9.5 wt% (Table 1).

Table 2 CO_2 adsorption data for various amine-functionalized SBA-15 and MSF samples

Sample	N content (mmol/g)	CO_2 uptake (mmol/g)	CO_2/N (mmol/mmol)
APS-SBA-15	4.0	0.8	0.20
TA-SBA-15	6.9	1.0	0.15
APS-MSF	3.4	0.8	0.24
TA-MSF	4.0	1.3	0.33
TEPA-MSFas-0.6	0.4	0.1	0.25
TEPA-MSFas-7.5	5.3	1.2	0.23
TEPA-MSFas-8.9	6.4	1.9	0.30
TEPA-MSFas-13.7	9.8	3.3	0.34
TEPA-MSFas-18.1	12.9	4.5	0.35

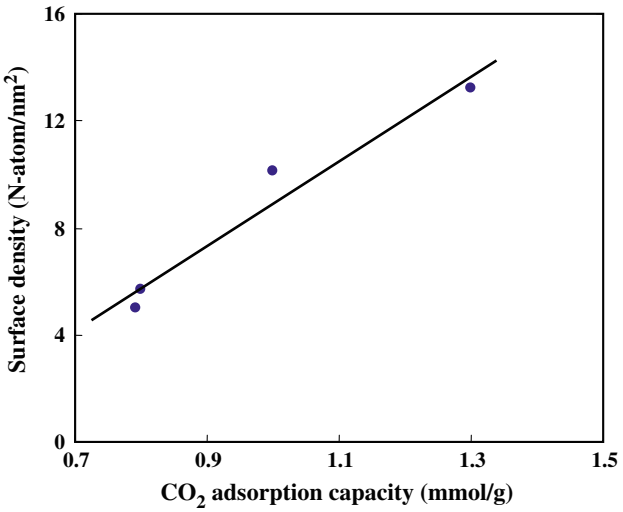

Fig. 4 Correlation of surface density of amine with CO_2 adsorption capacity for various amine-functionalized mesoporous silicas

The CO_2 adsorption capacities of various amino-functionalized SBA-15 and MSF are summarized in Table 2. Unlike the parent SBA-15 and MSF samples, which showed nearly null CO_2 uptake, amine-functionalized samples revealed a modest adsorption capacity of ca. 0.8–1.3 mmol/g. That the APS-functionalized silicas showed higher amine efficiencies (CO_2/N) than that of TA-functionalized samples may be attributed to the steric hindrance caused by the long organic chains. The correlation of CO_2 adsorption capacity with surface density of amine is shown in Fig. 4. It was found that CO_2 adsorption capacity is in proportion with the surface density of amine, whereas no obvious correlation between the CO_2 uptake and pore volume of the amine-functionalized adsorbents could be found.

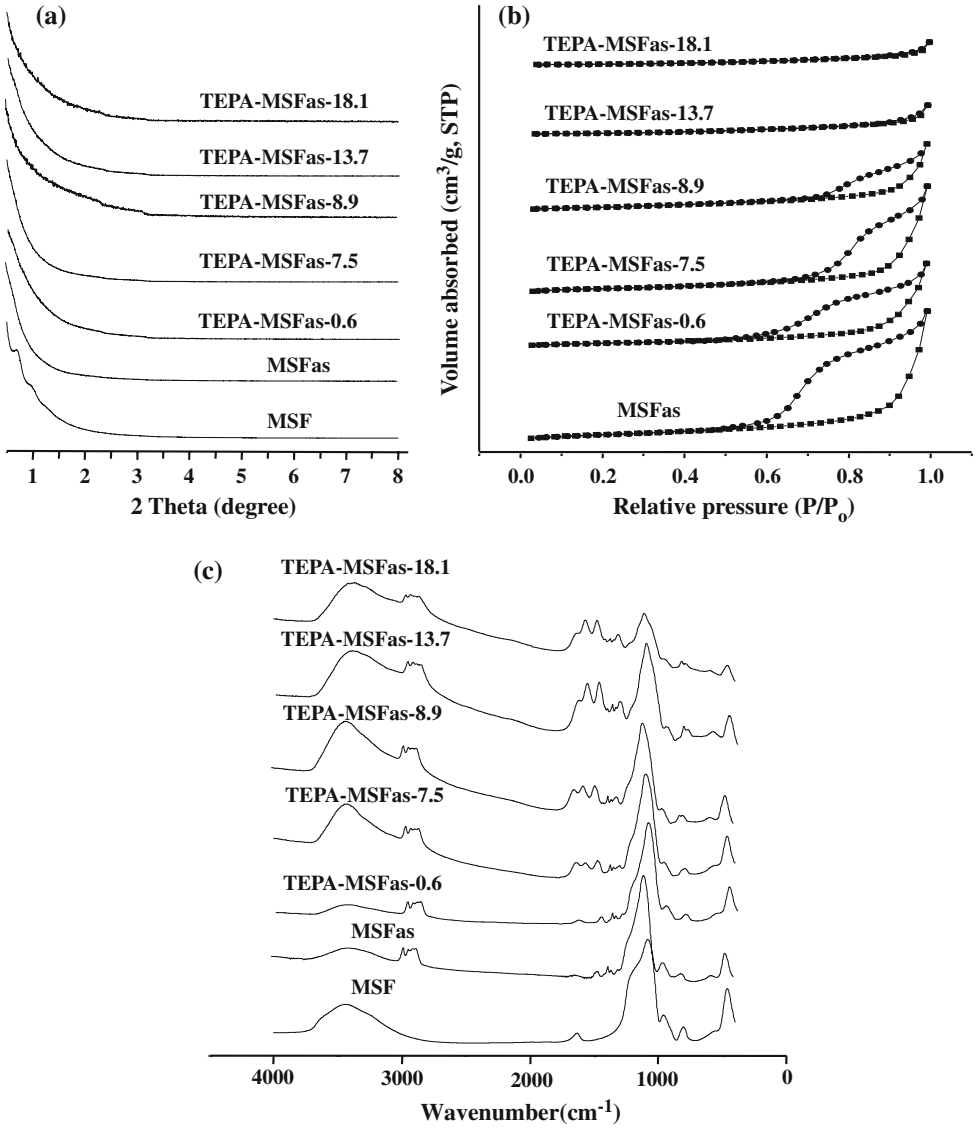

Fig. 5 **a** XRD patterns, **b** N_2 adsorption-desorption isotherms and **c** FTIR spectra of TEPA-MSFas-*x* samples

To increase the surface density of amine on the silica support, we incorporated different amounts of TEPA into the as-synthesized MSF. Small angle XRD patterns in Fig. 5a revealed that the structure of MSF remained practically intact regardless of the amount of TEPA introduced. Upon increasing TEPA loading, progressive decreases in N_2 adsorption amounts and hysteresis loops (Fig. 5b) were evident. The FTIR spectra in Fig. 5c also revealed the presence of amine compounds in the TEPA-MSFas-*x* samples, as evidenced by the absorption bands near 1510 cm^{-1}. Further quantitative measurements by elemental analysis showed that the nitrogen contents in these samples range from 0.6 to 18.1 wt%, as shown in Table 1.

The effects of TEPA loading amount on CO_2 adsorption capacity and amine efficiency (CO_2/N) of various TEPA-MSFas-*x* absorbents are summarized in Table 2. It is obvious that both CO_2 adsorption capacity and amine efficiency (CO_2/N) of the composite increase with increasing amount of TEPA loaded on as-synthesized MSF. Again, this may be attributed to the increase in the surface density of amine on TEPA-MSFas-*x* (see Fig. 6) with increasing N content (*x*). It is indicative that densely anchored aminosilanes would be more effective as adsorption site than those isolated on bare silica supports. As a result, the TEPA-MSFas-18.1 sample exhibited a remarkably high CO_2 adsorption capacity of 4.5 mmol/g. surpassing the value of ca. 3.9 mmol/g reported for TEPA (ca. 70 wt%) modified on as-synthesized SBA-15 [56]. In fact, we also performed similar experiments on a series of as-synthesized SBA-15 (not shown). With a modest TEPA loading (ca. 16.3 wt%, corresponding to N content of 11.6 mmol/g), we were able to obtain a CO_2 adsorption capacity of ca. 4.5 mmol/g, which is corresponding to an amine efficiency of 0.39 mmol/mmol. Further investigations have been undertaken to resolve the detailed chemical adsorption mechanism involved in CO_2 adsorption on

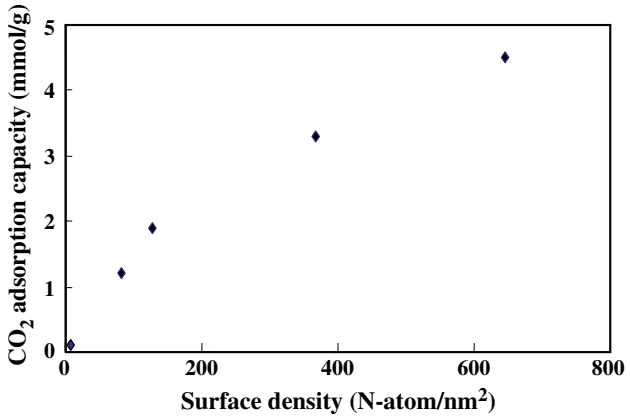

Fig. 6 Variations of CO_2 adsorption capacity with surface density of amine observed for various TEPA-MSFas-*x* samples

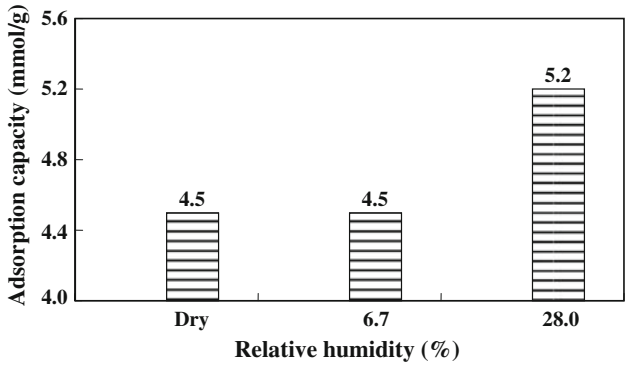

Fig. 7 Effect of moisture concentrations on CO_2 adsorption capacity for the TEPA-MSFas-18.1 sample

these organic template occluded mesoporous silica-amine composites.

For practical industrial applications in CO_2 capture, solid adsorbents should possess not only high adsorptive capacity for CO_2 with moisture, but also stable cyclic adsorption-desorption performance during long-term operation. The effect of moisture concentration in the flue gas on CO_2 adsorption of the TEPA-MSFas-18.1 sample was examined, as shown in Fig. 7. It was found that CO_2 adsorption capacity tends to increase with increasing moisture concentration in the simulated 15% CO_2 flue gas. An enhanced CO_2 adsorption capacity of ca. 5.3 mmol/g was obtained under the exposure of 28% relative humidity, which is ca. 18% higher than that obtained from simulated dry flue gas. It should be noted that the CO_2 adsorption capacity of TEPA-MSFas-18.1 in the nineth adsorption cycle (i.e., total operation period of ca. 18 h, Fig. 8) under dry 15% CO_2 concentration remains at ca. 3.6 mmol/g, which is still higher than the benchmark value for commercialization (2.0 mmol/g).

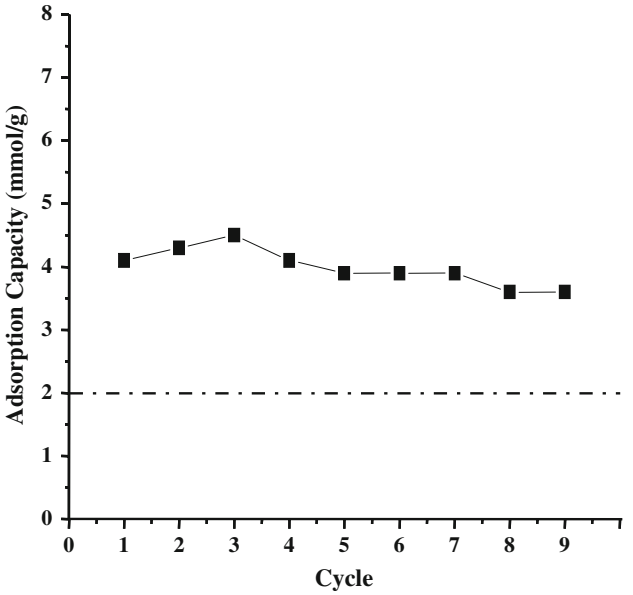

Fig. 8 Cyclic CO_2 adsorption tests of TEPA-MSFas-18.1 sample at 348 K. The *dashed line* indicates the benchmark value for commercialization

4 Conclusions

CO_2 uptake measurements on amine (TA, APS)-functionalized silica (SBA-15 and MSF) prepared by a post-synthesis grafting method showed that while the CO_2 adsorption capacity increase with increasing surface density of amine, no obvious correlation between the CO_2 uptake and pore volume of the amine-functionalized adsorbents could be found. However, owing to the difficulty in loading excessive amount of amine, these materials typically reach a maximum CO_2 adsorption capacity less than ca. 1.3 mmol/g at 348 K under ambient pressure using dry 15% CO_2, which is less than the benchmark value ($\sim$2.0 mmol/g) for commercialization. On the other hand, by directly incorporating TEPA onto the as-synthesized MSF in the presence of organic template, the TEPA-MSFas-18.1 absorbent so prepared was found to reach a remarkable CO_2 adsorption capacity of ca. 4.5 mmol/g. Such drastic enhancement in CO_2 uptake compared to the amine-functionalized silicas without template is ascribed due to the increase in surface density of amine. Under the exposure of 28% relative humidity, the TEPA-MSFas-18.1 sample revealed a further increase in CO_2 adsorption capacity to 5.2 mmol/g, surpassing that of other solid adsorbents. Furthermore, the absorbent remains active after repeated adsorption-desorption cycles, revealing a new opportunity for future practical applications and commercialization.

Acknowledgments The support of this work by the National Science Council, Taiwan (NSC95-2113-M-001-040-MY3) is gratefully

acknowledged. The authors thank Drs. Shing-Jong Huang and Ningya Yu for helpful discussions.

References

1. Song C (2006) Catal Today 115:2
2. Figueroa JD, Fout T, Plasynski S, Mcllvried H, Srivastava RD (2008) Int J Greenh Gas Control 2:9
3. Morris RE, Wheatley PS (2008) Angew Chem Int Ed 47:4966
4. Satyapal S, Filburn T, Trela J, Strange J (2001) Energy Fuels 15:250
5. Rinker E, Ashour SS, Sandall OC (2000) Ind Eng Chem Res 39:4346
6. Little RJ, Versteeg GF, Van Swaaij WPM (1992) Chem Eng Sci 47:2027
7. Veawab A, Tontiwachwuthikul P, Chakma A (1999) Ind Eng Chem Res 38:3917
8. Hook RJ (1997) Ind Eng Chem Res 36:1779
9. Jensen MB, Petersson LGM, Swang O, Olsbye U (2005) J Phys Chem B 109:16774
10. Feng B, Liu W, Li X, An H (2006) Energy Fuel 20:2417
11. Mosqueda HA, Bazquez C, Bosch P, Pfeiffer H (2006) Chem Mater 18:2307
12. Ebner AD, Reynolds SP, Ritter JA (2006) Ind Eng Chem Res 45:6378
13. Essaki K, Nakagawa K, Kato M (2004) J Chem Eng Jpn 37:772
14. Kato M, Essaki K, Yoshikawa S, Nakagawa K, Uemoto H (2004) J Ceram Soc Jpn 112:S1338
15. Pfeiffer H, Bosch P (2005) Chem Mater 17:1704
16. Ochoa-Fernández E, Rønning M, Grande T, Chen D (2006) Chem Mater 18:6037
17. Venegas MJ, Fregoso-Israel E, Escamilla R, Pfeiffer H (2007) Ind Eng Chem Res 46:2407
18. Tang J, Tang H, Sun W, Radosz M, Shen Y (2005) J Polym Sci A 43:5477
19. Zhang J, Zhang S, Dong K, Zhang Y, Shen Y, Lv X (2006) Chem Eur J 12:4021
20. Himeno S, Tomita T, Suzuki K, Yoshida S (2007) Microporous Mesoporous Mater 98:62
21. Li P, Tezel H (2007) Microporous Mesoporous Mater 98:94
22. Maurin G, Bell R, Kuchta B, Poyet T, Llewellyn P (2005) Adsorption 11:331
23. Siriwardance RV, Shen MS, Fisher EP (2005) Energy Fuels 19:1153
24. Walton KS, Abney MB, LeVan MD (2006) Microporous Mesoporous Mater 91:78
25. Pulido A, Nachtigall P, Zukal A, Domínguez I, Čejka J (2009) J Phys Chem C 113:2928
26. Zukal A, Pawlesa J, Čejka J (2009) Adsorption 15:264
27. Himeno S, Komatsu T, Fujita S (2005) J Chem Eng Data 50:369
28. Omi H, Ueda T, Miyakubo K, Eguchi T (2005) Appl Surf Sci 252:660
29. Arenillas A, Smith KM, Drage TC, Snape CE (2005) Fuel 84:2204
30. Larobina D, Sanguigno L, Venditto V, Guerra G, Mensitieri G (2004) Polymer 45:429
31. Navarro JAR, Barea E, Salas JM, Masciocchi N, Galli S, Sironi A, Ania CO, Parra JB (2006) Inorg Chem 45:2397
32. Thallapally PK, McGrail BP, Atwood JL, Gaeta C, Tedesco C, Neri P (2007) Chem Mater 19:3355
33. Brandani F, Ruthven DM (2004) Ind Eng Chem Res 43:8339
34. Li H, Eddaoudi M, Groy TL, Yaghi OM (1998) J Am Chem Soc 120:8571
35. Walton KS, Millward AR, Dubbeldam D, Frost H, Low JJ, Yaghi OM, Snurr RQ (2008) J Am Chem Soc 130:406
36. Serre C, Millange F, Thouvenot C, Nogues M, Marsolier G, Louer D, Férey G (2002) J Am Chem Soc 124:13519
37. Serre C, Bourrelly S, Vimont A, Ramsahye NA, Maurin G, Llewellyn PL, Daturi M, Filinchuk Y, Leynaud O, Barnes P, Férey G (2007) Chem Mater 19:2246
38. Sozzani P, Bracco S, Comotti A, Ferretti L, Simonutti R (2005) Angew Chem Int Ed 44:1816
39. Liu X, Li J, Zhou L, Huang D, Zhou Y (2005) Chem Phys Lett 415:198
40. Khatri RA, Chuang SSC, Soong Y, Gray M (2005) Ind Eng Chem Res 44:3702
41. Zheng F, Tran DN, Busche BJ, Fryxell GE, Addleman RS, Zemanian TS, Ardahl CL (2005) Ind Eng Chem Res 44:3099
42. Macario A, Katovic A, Giordano G, Iucolano F, Caputo D (2005) Microporous Mesoporous Mater 81:139
43. Xu X, Song CS, Andresen JM, Miller BG, Scaroni AW (2002) Energy Fuels 16:1463
44. Xu X, Song CS, Andresen JM, Miller BG, Scaroni AW (2003) Microporous Mesoporous Mater 62:29
45. Xu X, Song CS, Miller BG, Scaroni AW (2005) Fuel Proc Technol 86:1457
46. Xu X, Song CS, Miller BG, Scaroni AW (2005) Ind Eng Chem Res 44:8113
47. Zeleňák V, Badaničová M, Halamová D, Čejka J, Zukal A, Murafa N, Goerigk G (2008) Chem Eng J 144:336
48. Kim S, Ida J, Guliants VV, Lin JYS (2005) J Phys Chem B 109:6287
49. Knowles GP, Graham JC, Delaney SW, Chaffee AL (2005) Fuel Proc Technol 86:1435
50. Knowles GP, Delaney SW, Chaffee AL (2006) Ind Eng Chem Res 45:2626
51. Hiyoshi N, Yogo K, Yashima T (2005) Microporous Mesoporous Mater 84:357
52. Liu X, Zhou L, Fu Z, Sun Y, Su W, Zhou Y (2007) Chem Eng Sci 62:1101
53. Knöfel C, Descarpentries J, Benzaouia A, Zeleňák V, Mornet S, Llewellyn PL, Hornebecq V (2007) Microporous Mesoporous Mater 99:79
54. Chang ACC, Chuang SSC, Gray M, Soong Y (2003) Energy Fuels 17:468
55. Gray ML, Soong Y, Champagne KJ, Pennline HW, Baltrus J, Stevens RWJ, Khatri RA, Chuang SSC, Filburn T (2005) Fuel Proc Technol 86:1449
56. Khatri RA, Chuang SSC, Soong Y, Gray M (2006) Energy Fuels 20:1514
57. Yue MB, Chun Y, Cao Y, Dong X, Zhu JH (2006) Adv Funct Mater 16:1717
58. Hicks JC, Drese JH, Fauth DJ, Gray ML, Qi G, Jones CW (2008) J Am Chem Soc 130:2902
59. Franchi RS, Harlick PJE, Sayari A (2005) Ind Eng Chem Res 44:8007
60. Reynhardt JPK, Yang Y, Sayari A, Alper H (2005) Adv Funct Mater 15:1641
61. Harlick PJE, Sayari A (2006) Ind Eng Chem Res 45:3248
62. Harlick PJE, Sayari A (2007) Ind Eng Chem Res 46:446
63. Serna-Guerrero R, Da'na E, Sayari A (2008) Ind Eng Chem Res 47:9406
64. Zhao D, Feng J, Huo Q, Melosh N, Fredrickson GH, Chmelka BF, Stucky GD (1998) Science 279:548
65. Lee J, Sohn K, Hyeon T (2001) J Am Chem Soc 123:5146